ACS APPLIED MATERIALS & INTERFACES

Research Article

www.acsami.org

Free-Standing $Na_{2/3}Fe_{1/2}Mn_{1/2}O_2$@Graphene Film for a Sodium-Ion Battery Cathode

Hongli Zhu,[†] Kang Taek Lee,[†,‡] Gregory Thomas Hitz,[†] Xiaogang Han,[†] Yuanyuan Li,[†] Jiayu Wan,[†] Steven Lacey,[†] Arthur von Wald Cresce,[§] Kang Xu,*[,§] Eric Wachsman,*[,†] and Liangbing Hu*[,†]

[†]Department of Materials Science and Engineering, University of Maryland, College Park, Maryland 20742, United States

[‡]Department of Energy Systems Engineering, Daegu Gyeongbuk Institute of Science and Technology (DGIST), 50-1 Sang-Ri, Hyeonpung-Myeon, Dalseong-Gun, Daegu 711-873, Korea

[§]U.S. Army Research Laboratory, Adelphi, Maryland 20783, United States

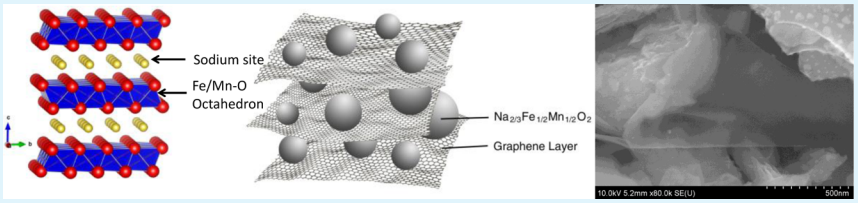

ABSTRACT: The development of high-performance cathodes for sodium-ion batteries remains a great challenge, while low-cost, high-capacity $Na_{2/3}Fe_{1/2}Mn_{1/2}O_2$ is an attractive electrode material candidate comprised of earth-abundant elements. In this work, we designed and fabricated a free-standing, binder-free $Na_{2/3}Fe_{1/2}Mn_{1/2}O_2$@graphene composite via a filtration process. The porous composite led to excellent electrochemical performance due to the facile transport for electrons and ions that was characterized by electrochemical impedance spectroscopy at different temperatures. The electrode delivered a reversible capacity of 156 mAh/g with high Coulombic efficiency. The importance of a fluorinated electrolyte additive with respect to the performance of this high-voltage cathode in Na-ion batteries was also investigated.

KEYWORDS: *Na-ion battery cathode, $Na_{2/3}Fe_{1/2}Mn_{1/2}O_2$, graphene, free-standing, electrolyte, binder-free*

INTRODUCTION

Electrochemical storage devices are indispensable components in renewable energy systems used to collect energy from intermittent sources such as solar and wind power. Compared to those of battery chemistries developed for electric vehicles, the most critical requirement for these grid-scale stationary storage devices is low cost ($100/kWh) instead of high energy density, in sharp contrast to the requirements for portable electronics and automotive applications.[1,2] Other desirable qualities for grid-scale energy storage include safely and efficiently capturing and releasing energy, low environmental impact, high power density, high round trip efficiency (RTE), long cycle and calendar life, and demonstrating wide service temperature ranges.[3]

Currently, only two energy storage technologies meet the cost target mentioned above: pumped hydroelectric storage and subsurface compressed air energy storage.[1,4] However, their extensive deployment is impractical because both are restricted to certain geographic locations, which brings compounded costs for transmission and distribution. High-electrochemical potential and low-cost Na-ion battery (NIB) technology utilizing earth-abundant materials thus emerges as a viable energy storage alternative to meet the grid storage requirements mentioned above.[5,6] For this nascent chemistry to work, rational structural designs for the effective manipulation of the transport of electrons and ions across multiporous electrodes are essential.

Various NIB materials have been demonstrated as anodes and cathodes, the former including $Na_2C_8H_4O_4$, $Li_4Ti_5O_{12}$, $Na_{0.66}Li_{0.22}Ti_{0.78}O_2$, hard carbon, porous hollow carbon spheres and tubes, and tin and its alloys[7−12] and the latter including bilayer $Na_2V_2O_5$, P2-$Na_{2/3}Fe_{1/2}Mn_{1/2}O_2$, $Na_3V_2(PO_4)_3$, $NaMn_{1/3}Co_{1/3}Ni_{1/3}PO_4$, etc.[8,10,13−20] Among all these cathode materials, $Na_{2/3}Fe_{1/2}Mn_{1/2}O_2$ is particularly attractive because it provides high capacity while entirely consisting earth-abundant elements.[3] In a recent report, Yabuuchi designed composite electrodes based on P2-$Na_{2/3}Fe_{1/2}Mn_{1/2}O_2$ and carbon black, demonstrating a performance breakthrough in NIB technology.[11] However, the presence of inert carbon black in the composite decreases the effective mass of the electrode and lowers the energy density on a full cell level. Furthermore, *N*-methyl-2-pyrrolidone (NMP), a solvent commonly used in battery processing while well-known for its negative environmental impact, has to be used for the reported electrode coating. For the large-scale production of consumer batteries, NMP already casts doubt on the sustainability; grid-storage applications are usually on the megawatt scale, which would

Received: December 25, 2013
Accepted: March 3, 2014
Published: March 3, 2014

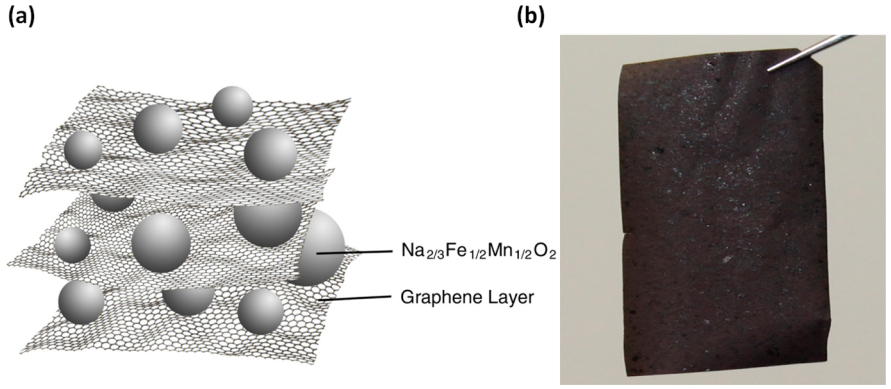

Figure 1. (a) Schematic of the $Na_{2/3}Fe_{1/2}Mn_{1/2}O_2$@graphene film. (b) Digital image of a free-standing film based on the $Na_{2/3}Fe_{1/2}Mn_{1/2}O_2$@graphene composite.

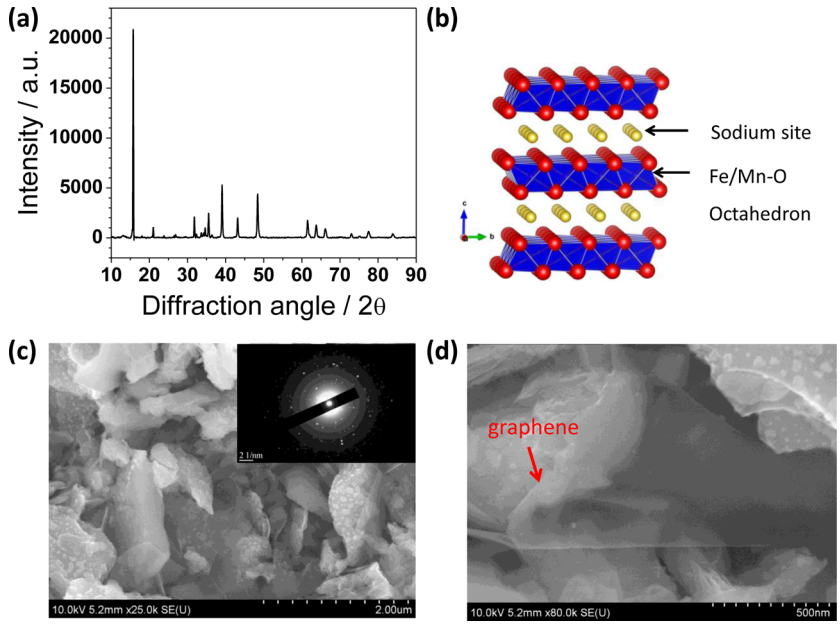

Figure 2. (a) X-ray diffraction spectroscopy of P2 phase $Na_{2/3}Fe_{1/2}Mn_{1/2}O_2$. (b) Schematic of the P2-$Na_{2/3}Fe_{1/2}Mn_{1/2}O_2$ structure. (c) SEM image of the electrode material mixed with graphene. The inset is the TEM diffraction pattern of graphene. (d) SEM image of the composite electrode before electrochemical testing.

cause greater concern only if such adverse materials were required. A greener process is therefore necessary to deploy sustainable grid-scale energy storage electrode materials in commercially viable battery technologies.

In this work, we address these issues by designing a process to prepare a promising NIB cathode material using a scalable filtration method based on aqueous ink. This process was used to design a nanocomposite electrode of $Na_{2/3}Fe_{1/2}Mn_{1/2}O_2$ with surfactant-free graphene flakes.[21] Electrochemical impedance spectroscopy (EIS) was used to study the ion and electron transport within the composite electrode at various temperatures, and the effect of different electrolytes, especially fluorinated solvent additives, was also investigated.

RESULTS AND DISCUSSION

Graphene is a well-known material endowed with numerous advantages that have led to its extensive use as a conductive additive in Li-ion batteries, including superior electronic conductivity, a large surface area, and excellent mechanical strength.[22−24] A schematic shown in Figure 1a depicts a composite material comprised of 10 wt % graphene and 90 wt % $Na_{2/3}Mn_{1/2}Fe_{1/2}O_2$ particles in which the two-dimensional graphene sheets serve as the scaffold for the various active particles to form a three-dimensional (3D) network for electron transport. The homogeneous distribution of $Na_{2/3}Mn_{1/2}Fe_{1/2}$-O_2 particles within this 3D conducting matrix minimizes the distances that the electrons must travel for the redox reaction to occur. The Na^+ storage capacity of such a composite film based on $Na_{2/3}Mn_{1/2}Fe_{1/2}O_2$@graphene is expected to be fully utilized while rapidly capturing and releasing charges. Additionally, the composite's porous structure would favor electrolyte penetration and ion transport. Using the previously $Na_{2/3}Mn_{1/2}Fe_{1/2}O_2$ and graphene, a free-standing, binder-free electrode shown in Figure 1b, was prepared by a solution-based vacuum filtration process.

There are two classifications of sodium-based layered electrode materials: O3 and P2 phases in which sodium ions are accommodated at octahedral and prismatic sites, respectively.[25] The X-ray diffraction (XRD) pattern for crystalline $Na_{2/3}Fe_{1/2}Mn_{1/2}O_2$ is shown in Figure 2a, where all the diffraction lines are indexed to a hexagonal lattice that is

dx.doi.org/10.1021/am405970s | ACS Appl. Mater. Interfaces 2014, 6, 4242−4247

characteristic of a P2-type layered phase.[26] The schematic structure of $Na_{2/3}Fe_{1/2}Mn_{1/2}O_2$ is shown in Figure 2b, where a Na^+ is accommodated at the prismatic site between two layered octahedral MnO_2 molecules. A longer interlayer distance is observed for the P2 phase because of the repulsive electrostatic interaction of the AA-type oxygen stacking that forms the prismatic sites.[14,27,28] Meanwhile, the P2 lattice is more stable because of its narrow gallery spacing and relatively immobile pillaring alkali ions. The stronger pillaring effect imparts structural stability, which is reflected by the electrochemical reversibility of this material.[26] The field emission scanning electron microscopy (FESEM) images shown in panels c and d of Figure 2 reveal that the particle size of the $Na_{2/3}Fe_{1/2}Mn_{1/2}O_2$ material synthesized in this work is approximately 500 nm. Thorough mixing of the $Na_{2/3}Fe_{1/2}Mn_{1/2}O_2$ particles and graphene plates as well as a highly crystalline graphene lattice was identified in the SEM and transmission electron microscopy (TEM) images, Figure 2c. It is expected that in such a nanostructure, electrons can travel submicrometer distances without scattering in the graphene to provide excellent electronic conductivity for the electrode.[29] In Figure 2d, one can visualize a single sheet of graphene with a high aspect ratio. Because of the large aspect ratio of the graphene flakes, a low percolation threshold is needed to achieve an excellent 3D conductive network. Conductivity measurements placed the typical resistance of the free-standing film of $Na_{2/3}Fe_{1/2}Mn_{1/2}O_2$@graphene mentioned above is around 200 Ω, indicating a well-wired composite.

The electrical conductivity of $Na_{2/3}Fe_{1/2}Mn_{1/2}O_2$ was investigated using the AC impedance technique at various temperatures. Figure 3a–c shows the typical Nyquist plots

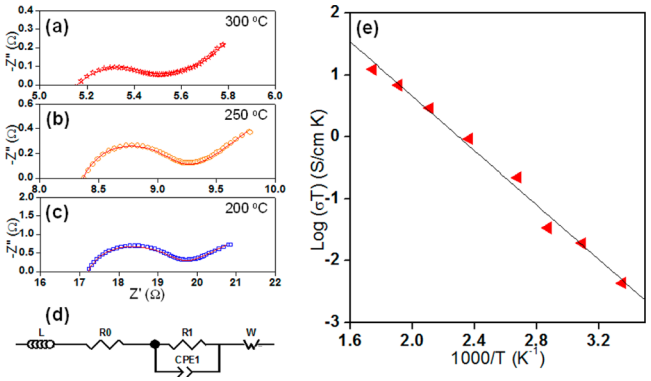

Figure 3. Typical Nyquist plots obtained for $Na_{2/3}Fe_{1/2}Mn_{1/2}O_2$ in air at (a) 300 °C (red stars), (b) 250 °C (orange circles), and (c) 200 °C (blue squares) using a Ag|$Na_{2/3}Fe_{1/2}Mn_{1/2}O_2$|Ag symmetric cell over the frequency range from 1 MHz to 0.1 Hz. (d) Equivalent circuit. The solid lines in panels a–c represent the fitted results using the equivalent circuit. (e) Arrhenius plot for the total electrical conductivity of $Na_{2/3}Fe_{1/2}Mn_{1/2}O_2$ measured from 25 to 300 °C.

obtained at various temperatures for the Ag|$Na_{2/3}Fe_{1/2}Mn_{1/2}O_2$|Ag symmetric cell. The measured impedance spectra were deconvoluted by Z-plot software using an equivalent circuit shown in Figure 3d. In the equivalent circuit, L, R_o, R_1, CPE_1, and W represent the inductance, bulk resistance, grain boundary resistance, constant phase element, and Warburg element for an air electrode, respectively. The resultant fit using the equivalent circuit was also overlapped in the impedance spectra shown in Figure 3a–c. From these results, the electrical conductivity of $Na_{2/3}Fe_{1/2}Mn_{1/2}O_2$ was determined by the sum of the bulk and grain boundary resistances (R_o + R_1) normalized by the sample's geometry (11.64 mm diameter; 1.26 mm height).

Figure 3e shows the Arrhenius plot for the electrical conductivity of the $Na_{2/3}Fe_{1/2}Mn_{1/2}O_2$ material with a Ag electrode. The measured total electrical conductivities of the sample, which includes contributions from the mobility of both electrons and ions, were 1.47×10^{-5}, 5.88×10^{-5}, 5.92×10^{-4}, 6.12×10^{-3}, and 2.15×10^{-2} S/cm at 25, 50, 100, 200, and 300 °C, respectively. The temperature dependence of the electrical conductivity is expressed by the Arrhenius equation:

$$\sigma = \frac{A}{T} \exp\left(-\frac{E_a}{kT}\right) \quad (1)$$

where σ, A, T, k, and E_a represent the electrical conductivity, pre-exponential factor, absolute temperature, Boltzmann's constant, and activation energy, respectively. Via application of eq 1 to the data shown in Figure 3e, the activation energy was calculated to be approximately 0.44 eV, which is comparable to the reported values for $Na_{0.44}Mn_{1-x}Ti_xO_2$ cathodes (0.38–0.53 eV).[30]

Electrochemical half-cells with $Na_{2/3}Fe_{1/2}Mn_{1/2}O_2$@graphene composites were assembled against a metallic sodium counter electrode and tested in an electrolyte consisting of 1.0 M $NaClO_4$ in propylene carbonate (PC) using 2 vol % fluorinated ethylene carbonate (FEC) as the electrolyte additive. Figure 4a shows the voltage profiles of half-cells at a rate of 0.1 C, while Figure 4b shows their Coulombic efficiency (CE). Two plateaus at 2.25 and 4.10 V were observed, and the electrode material demonstrated a first discharge capacity of 156 mAh/g. The CE increased to 99% from the fourth cycle, indicating a reversible electrochemical intercalation of Na^+. The specific discharge capacity versus cycle number was plotted in Figure 4c, which shows fairly extensive capacity fading with cycling; however, the specific capacity still remains higher than those of most NIB cathode materials.[31−33]

To understand the cycling stability, EIS data was collected on half-cells stabilized at the same charged state (4.3 V) within a frequency range from 1 MHz to 100 mHz with an amplitude of 5 mV. At high frequencies, the intercept of the spectrum and the real axis is internal resistance R_s, which includes the electrolyte resistance, the intrinsic electrode resistance, and the contact resistance at the interface between the electrode and the current collector comprised of a CNT thin film. The semicircle at the high- to middle-frequency range represents charge transfer resistance R_{ct}. As shown in Figure 4d, R_s experiences a small change from 64 to 75 Ω after 60 cycles. Meanwhile, the semicircle remains fairly constant, indicating negligible changes in morphology and electronic structure in the electrode materials during cycling.

We also evaluated the effect of fluorinated electrolyte additives on the electrochemical performance of this $Na_{2/3}Fe_{1/2}Mn_{1/2}O_2$@graphene cathode material for Na-ion batteries. $NaPF_6$ (1.0 M) dissolved in ethylene carbonate (EC) and diethyl carbonate (DEC) (1:1 EC:DEC ratio by volume) was used as the reference to compare with the test electrolyte (1.0 M $NaPF_6$ in PC with 2% FEC). The $Na_{2/3}Fe_{1/2}Mn_{1/2}O_2$@graphene electrodes were fabricated, and the samples with identical parameters were evaluated. The results demonstrated a substantial difference in electrochemical performance when the fluorinated solvent additive was present. Figure 5a shows the voltage profile of the baseline electrolyte

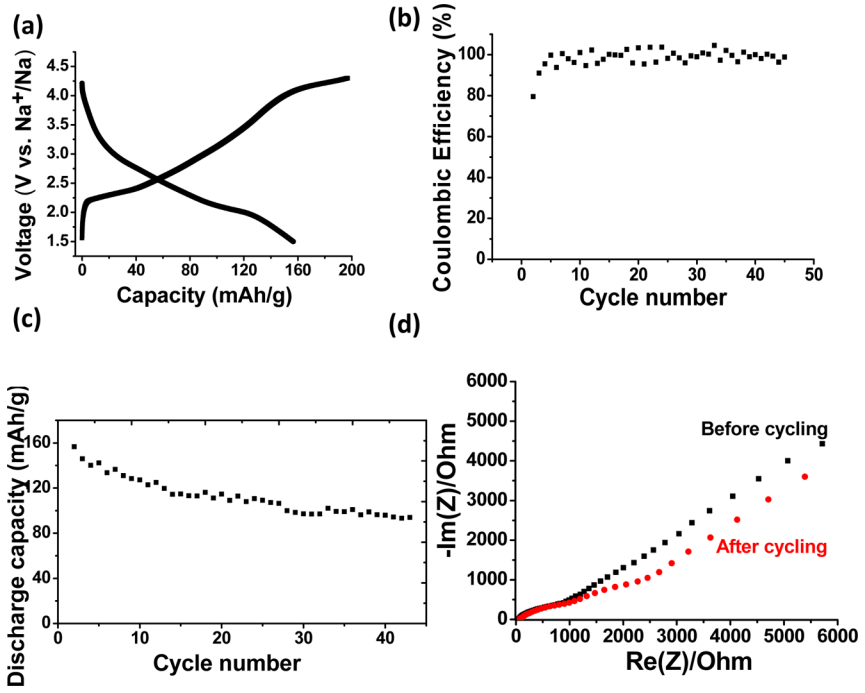

Figure 4. Electrode performance of P2 phase $Na_{2/3}Fe_{1/2}Mn_{1/2}O_2$ using 1.0 M $NaClO_4$ PC:FEC as the electrolyte. (a) Galvanostatic charge–discharge curve of the first cycle. Cells were tested in the voltage range from 1.5 to 4.3 V at a rate of 0.1 C. (b) Coulombic efficiency vs cycle number. (c) Discharge capacity at different cycles. (d) EIS data collected from a cell consisting of P2-$Na_{2/3}Fe_{1/2}Mn_{1/2}O_2$ mixed with graphene in 1.0 M $NaClO_4$ PC:FEC. The scan frequency was 1 MHz to 100 mHz.

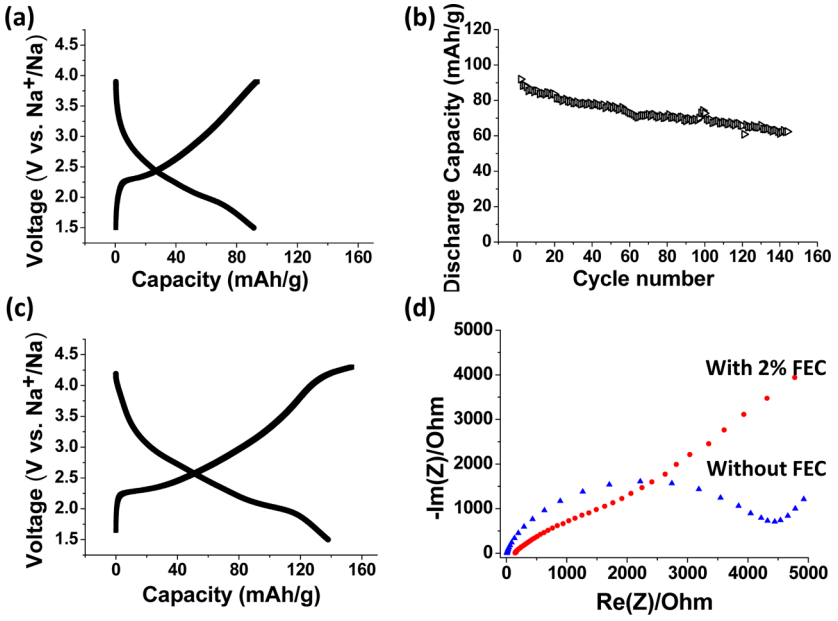

Figure 5. Influence of fluorinated ethylene carbonate (FEC) as an electrolyte additive for rechargeable Na batteries. (a) Voltage profile of P2-$Na_{2/3}Fe_{1/2}Mn_{1/2}O_2$ with 1.0 M $NaPF_6$ EC:DEC as the electrolyte at a rate of 0.1 C in the first cycle. (b) Cell cycling performance of P2-$Na_{2/3}Fe_{1/2}Mn_{1/2}O_2$ with 1.0 M $NaPF_6$ EC:DEC as the electrolyte at a rate of 0.1 C. (c) Voltage profile of P2-$Na_{2/3}Fe_{1/2}Mn_{1/2}O_2$ with 1.0 M $NaPF_6$ PC:FEC as the electrolyte at a rate of 0.1 C in the first cycle. (d) EIS curve comparison of P2-$Na_{2/3}Fe_{1/2}Mn_{1/2}O_2$ with two different electrolytes: 1.0 M $NaPF_6$ EC:DEC and 1.0 M $NaPF_6$ PC:FEC. Both cells were tested at a potential of 2.5 V to Na^+/Na.

with a stability window up to 3.9 V. In panels a and c of Figure 4 and panel a of Figure 5, a different electrolyte was used. On the basis of our study, we found that the electrolyte plays an important role for the sodium-ion battery. In Figure 4, the cell with 2% FEC electrolyte demonstrated stable charge–discharge performance up to 4.3 V. In Figure 5a, we used the electrolyte without FEC as the control sample. In this case, the electrolyte decomposed dramatically and the electrode cannot be charged above 3.9 V. Thus, the specific capacity accessed in Figure 5a is much smaller than what should be stored by $Na_{2/3}Fe_{1/2}Mn_{1/2}O_2$, as evidenced by the 90 mAh/g initial discharge capacity for the first cycle. That is the reason why the initial discharge capacity in panel a of Figure 5 is much lower than in panels a and c of Figure 4. After 140 cycles, the remaining discharge

dx.doi.org/10.1021/am405970s | ACS Appl. Mater. Interfaces 2014, 6, 4242–4247

capacity is 60 mAh/g (Figure 5b). However, the cycling stability of $Na_{2/3}Fe_{1/2}Mn_{1/2}O_2$ charged to 3.9 V is better than when it is charged to 4.3 V because of the more stable electrode structure. With only 2% FEC as shown in Figure 5c, the cathode−electrolyte interface was stabilized, and the assembled composite cell could be charged to 4.3 V with the second plateau at 4.1 V, which released additional capacity equal to 138 mAh/g. The interface plays an important role in sodium-ion batteries.[34,35] We speculate that the FEC additive formed a distinctly different interfacial chemistry on the cathode surface that allowed sodium intercalation at higher voltages. On the basis of the existing understanding of FEC's electrochemical behavior, it is more than likely there is oxidative breakdown on the cathode in the first cycle leaving behind an F-containing SEI layer.[36] Figure 5d shows the cell's EIS data at the same open circuit voltage (2.5 V). A substantial difference was observed between the cells with the baseline electrolyte and the corresponding FEC-containing electrolyte. FEC seems to demonstrate better electrochemical performance while having a much lower charge transfer resistance. We believe that this fluorinated electrolyte additive plays an important role in high-voltage cathode materials for Na-ion battery, and it merits more detailed investigation to decipher the precise reasoning behind the phenomenon mentioned above.

CONCLUSION

We successfully designed and fabricated a binder-free $Na_{2/3}Fe_{1/2}Mn_{1/2}O_2$@graphene composite with aqueous graphene ink via a scalable fabrication method. Such water-based process will be "greener" than the commonly adopted industry processes for coating electrodes with a PVDF binder in NMP solvents. The cell kinetics of this $Na_{2/3}Fe_{1/2}Mn_{1/2}O_2$@graphene composite were also investigated by EIS spectra at various temperatures, while studies of the effects of the electrolyte on cathode performance revealed the positive influence of fluorinated solvents with regard to sodium cells. This study can help design better cathodes and electrolytes for NIBs fabricated with scalable and more environmentally friendly processes.

EXPERIMENTAL SECTION

Powder Synthesis. $Na_{2/3}Fe_{1/2}Mn_{1/2}O_2$ was synthesized via a conventional solid state reaction.[11] The starting materials were Na_2O_2 (Sigma-Aldrich, 97%), Fe_2O_3 (Alfa Aesar, 99.945%), and MnO_2 (Alfa Aesar, 99.9%). The initial materials were mixed in stoichiometric proportions and ball milled for 24 h in ethanol. After being dried at 100 °C, the material was calcined for 12 h in an alumina crucible at 900 °C. The calcined powder was then ball milled once more for 24 h before being dried at 100 °C.

Characterization. The electrical conductivity of $Na_{2/3}Fe_{1/2}Mn_{1/2}O_2$ was measured by electrochemical impedance spectroscopy (EIS). The sample powder was pressed uniaxially into a pellet with a pressure of 132 MPa in a 13 mm diameter steel die before it was sintered for 8 h in an alumina crucible at 950 °C. Ag electrodes were deposited on both surfaces of the pellet by brush painting and were annealed at 750 °C for 1 h in air. Silver mesh attached to the platinum leads was embedded in the silver paste prior to sintering. The Ag|$Na_{2/3}Fe_{1/2}Mn_{1/2}O_2$|Ag symmetric cell was loaded on the quartz tube reactor and measured by two-point probe EIS using a Solartron 1260 instrument with an AC voltage amplitude of 50 mV over the frequency range from 1 MHz to 0.1 Hz in air. The temperature range was from 25 °C (room temperature) to 300 °C, and the cell was equilibrated at a constant temperature prior to each EIS measurement.

Free-Standing Electrode Preparation. $Na_{2/3}Fe_{1/2}Mn_{1/2}O_2$ (90 wt %) was mixed with 10 wt % graphene in deionized water and sonicated for 30 min. The suspension was then vacuum filtered using an anodic aluminum oxide (AAO) membrane. A thin layer of CNT was prefiltered as the current collector. The film peeled off automatically from the AAO after it dried.

Battery Assembly and Electrochemical Measurements. Half-cells composed of a $Na_{2/3}Fe_{1/2}Mn_{1/2}O_2$@graphene working electrode and solid Na metal (99%, Sigma-Alrich) counter electrode were assembled for electrochemical characterization. Separators and CR2032 coin cell cases were purchased from MTI, Inc. The electrochemical performance of the cells was tested using a Biologic VMP3 electrochemical potentiostat.

AUTHOR INFORMATION

Corresponding Authors

*E-mail: conrad.k.xu.civ@mail.mil.
*E-mail: binghu@umd.edu.
*E-mail: ewach@umd.edu.

Author Contributions

H.Z. and K.T.L. contributed equally to this work.

Notes

The authors declare no competing financial interest.

ACKNOWLEDGMENTS

L.H. acknowledges the startup support from the University of Maryland. We acknowledge the support of the Maryland Nanocenter as well as its Fablab and Nisplab.

REFERENCES

(1) Madlener, R.; Latz, J. Economics of centralized and decentralized compressed air energy storage for enhanced grid integration of wind power. *Appl. Energy* **2013**, *101*, 299−309.

(2) Yang, Z. G.; Zhang, J. L.; Kintner-Meyer, M. C. W.; Lu, X. C.; Choi, D. W.; Lemmon, J. P.; Liu, J. Electrochemical Energy Storage for Green Grid. *Chem. Rev.* **2011**, *111*, 3577−3613.

(3) Hayashi, A.; Noi, K.; Sakuda, A.; Tatsumisago, M. Superionic glass-ceramic electrolytes for room-temperature rechargeable sodium batteries. *Nat. Commun.* **2012**, *3*, Article No. 856.

(4) Connolly, D.; Lund, H.; Finn, P.; Mathiesen, B. V.; Leahy, M. Practical operation strategies for pumped hydroelectric energy storage (PHES) utilising electricity price arbitrage. *Energy Policy* **2011**, *39*, 4189−4196.

(5) Slater, M. D.; Kim, D.; Lee, E.; Johnson, C. S. Sodium-Ion Batteries. *Adv. Funct. Mater.* **2013**, *23*, 947−958.

(6) Pan, H.; Hu, Y.-S.; Chen, L. Room-temperature stationary sodium-ion batteries for large-scale electric energy storage. *Energy Environ. Sci.* **2013**, *6*, 2338−2360.

(7) Liu, Y.; Xu, Y.; Zhu, Y.; Culver, J. N.; Lundgren, C. A.; Xu, K.; Wang, C. Tin Coated Viral-Nanoforests as Sodium-Ion Battery Anodes. *ACS Nano* **2013**, *7*, 3627−3634.

(8) Komaba, S.; Murata, W.; Ishikawa, T.; Yabuuchi, N.; Ozeki, T.; Nakayama, T.; Ogata, A.; Gotoh, K.; Fujiwara, K. Electrochemical Na Insertion and Solid Electrolyte Interphase for Hard-Carbon Electrodes and Application to Na-Ion Batteries. *Adv. Funct. Mater.* **2011**, *21*, 3859−3867.

(9) Xiao, L.; Cao, Y.; Xiao, J.; Wang, W.; Kovarik, L.; Nie, Z.; Liu, J. High capacity, reversible alloying reactions in SnSb/C nanocomposites for Na-ion battery applications. *Chem. Commun.* **2012**, *48*, 3321−3323.

(10) Cao, Y.; Xiao, L.; Sushko, M. L.; Wang, W.; Schwenzer, B.; Xiao, J.; Nie, Z.; Saraf, L. V.; Yang, Z.; Liu, J. Sodium Ion Insertion in Hollow Carbon Nanowires for Battery Applications. *Nano Lett.* **2012**, *12*, 3783−3787.

(11) Zhao, L.; Zhao, J.; Hu, Y.-S.; Li, H.; Zhou, Z.; Armand, M.; Chen, L. Disodium Terephthalate ($Na_2C_8H_4O_4$) as High Performance Anode Material for Low-Cost Room-Temperature Sodium-Ion Battery. *Adv. Energy Mater.* **2012**, *2*, 962−965.

(12) Sun, Y.; Zhao, L.; Pan, H.; Lu, X.; Gu, L.; Hu, Y.-S.; Li, H.; Armand, M.; Ikuhara, Y.; Chen, L.; Huang, X. Direct atomic-scale confirmation of three-phase storage mechanism in $Li_4Ti_5O_{12}$ anodes for room-temperature sodium-ion batteries. *Nat. Commun.* **2013**, *4*, 1870.
(13) Tepavcevic, S.; Xiong, H.; Stamenkovic, V. R.; Zuo, X.; Balasubramanian, M.; Prakapenka, V. B.; Johnson, C. S.; Rajh, T. Nanostructured Bilayered Vanadium Oxide Electrodes for Rechargeable Sodium-Ion Batteries. *ACS Nano* **2012**, *6*, 530−538.
(14) Yabuuchi, N.; Kajiyama, M.; Iwatate, J.; Nishikawa, H.; Hitomi, S.; Okuyama, R.; Usui, R.; Yamada, Y.; Komaba, S. P2-type $Nax[Fe_{1/2}Mn_{1/2}]O_2$ made from earth-abundant elements for rechargeable Na batteries. *Nat. Mater.* **2012**, *11*, 512−517.
(15) Ponrouch, A.; Marchante, E.; Courty, M.; Tarascon, J.-M.; Rosa Palacin, M. In search of an optimized electrolyte for Na-ion batteries. *Energy Environ. Sci.* **2012**, *5*, 8572−8583.
(16) Abouimrane, A.; Weng, W.; Eltayeb, H.; Cui, Y. J.; Niklas, J.; Poluektov, O.; Amine, K. Sodium insertion in carboxylate based materials and their application in 3.6 V full sodium cells. *Energy Environ. Sci.* **2012**, *5*, 9632−9638.
(17) Kataoka, R.; Mukai, T.; Yoshizawa, A.; Sakai, T. Development of High Capacity Cathode Material for Sodium Ion Batteries $Na_{0.95}Li_{0.15}(Ni_{0.15}Mn_{0.55}Co_{0.1})O_2$. *J. Electrochem. Soc.* **2013**, *160*, A933−A939.
(18) Goodenough, J. B.; Song, J.; Xu, M.; Wang, L. Exploration of $NaVOPO_4$ as a Cathode for a Na-Ion Battery. *Chem. Commun.* **2013**, *49*, 5280−5282.
(19) Jian, Z.; Han, W.; Lu, X.; Yang, H.; Hu, Y.-S.; Zhou, J.; Zhou, Z.; Li, J.; Chen, W.; Chen, D.; Chen, L. Sodium-Ion Batteries: Superior Electrochemical Performance and Storage Mechanism of $Na_3V_2(PO_4)_3$ Cathode for Room-Temperature Sodium-Ion Batteries. *Adv. Energy Mater.* **2013**, *3*, 138−138.
(20) Wang, Y.; Yu, X.; Xu, S.; Bai, J.; Xiao, R.; Hu, Y.-S.; Li, H.; Yang, X.-Q.; Chen, L.; Huang, X. A zero-strain layered metal oxide as the negative electrode for long-life sodium-ion batteries. *Nat. Commun.* **2013**, *4*, Article No. 2365.
(21) Han, X.; Chen, Y.; Zhu, H.; Preston, C.; Wan, J.; Fang, Z.; Hu, L. Scalable, printable, surfactant-free graphene ink directly from graphite. *Nanotechnology* **2013**, *24*, 205304.
(22) Yoo, E.; Kim, J.; Hosono, E.; Zhou, H.-s.; Kudo, T.; Honma, I. Large Reversible Li Storage of Graphene Nanosheet Families for Use in Rechargeable Lithium Ion Batteries. *Nano Lett.* **2008**, *8*, 2277−2282.
(23) Wu, Z.-S.; Ren, W.; Wen, L.; Gao, L.; Zhao, J.; Chen, Z.; Zhou, G.; Li, F.; Cheng, H.-M. Graphene Anchored with Co_3O_4 Nanoparticles as Anode of Lithium Ion Batteries with Enhanced Reversible Capacity and Cyclic Performance. *ACS Nano* **2010**, *4*, 3187−3194.
(24) Wang, H.; Cui, L.-F.; Yang, Y.; Sanchez Casalongue, H.; Robinson, J. T.; Liang, Y.; Cui, Y.; Dai, H. Mn_3O_4-Graphene Hybrid as a High-Capacity Anode Material for Lithium Ion Batteries. *J. Am. Chem. Soc.* **2010**, *132*, 13978−13980.
(25) Delmas, C.; Fouassier, C.; Hagenmuller, P. Structural Classification and Properties of the Layered Oxides. *Physica B+C (Amsterdam)* **1980**, *99*, 81−85.
(26) Delmas, C.; Braconnier, J. J.; Fouassier, C.; Hagenmuller, P. Electrochemical Intercalation of Sodium in $NaxCOO_2$ Bronzes. *Solid State Ionics* **1981**, *3*−*4*, 165−169.
(27) Guignard, M.; Didier, C.; Darriet, J.; Bordet, P.; Elkaim, E.; Delmas, C. P2-$NaxVO_2$ system as electrodes for batteries and electron-correlated materials. *Nat. Mater.* **2013**, *12*, 74−80.
(28) Berthelot, R.; Carlier, D.; Delmas, C. Electrochemical investigation of the P2-$NaxCoO_2$ phase diagram. *Nat. Mater.* **2011**, *10*, 74.
(29) Meyer, J. C.; Geim, A.; Katsnelson, M.; Novoselov, K.; Booth, T.; Roth, S. The structure of suspended graphene sheets. *Nature* **2007**, *446*, 60−63.
(30) Funabiki, F.; Hayakawa, H.; Kijima, N.; Akimoto, J. Electrical Conductivities of $Na_{0.44}Mn_{1-x}Ti_xO_2$. *Electrochem. Solid-State Lett.* **2009**, *12*, F35−F38.
(31) Minakshi, M.; Meyrick, D. Reversible sodiation in maricite $NaMn_{1/3}Co_{1/3}Ni_{1/3}PO_4$ for renewable energy storage. *J. Alloys Compd.* **2013**, *555*, 10−15.
(32) Nose, M.; Nakayama, H.; Nobuhara, K.; Yamaguchi, H.; Nakanishi, S.; Iba, H. $Na_4Co_3(PO_4)_2P_2O_7$: A novel storage material for sodium-ion batteries. *J. Power Sources* **2013**, *234*, 175−179.
(33) Kim, H.; Shakoor, R. A.; Park, C.; Lim, S. Y.; Kim, J. S.; Jo, Y. N.; Cho, W.; Miyasaka, K.; Kahraman, R.; Jung, Y.; Choi, J. W. $Na_2FeP_2O_7$ as a Promising Iron-Based Pyrophosphate Cathode for Sodium Rechargeable Batteries: A Combined Experimental and Theoretical Study. *Adv. Funct. Mater.* **2013**, *23*, 1147−1155.
(34) Jian, Z.; Han, W.; Lu, X.; Yang, H.; Hu, Y.-S.; Zhou, J.; Zhou, Z.; Li, J.; Chen, W.; Chen, D.; Chen, L. Superior Electrochemical Performance and Storage Mechanism of $Na_3V_2(PO_4)_3$ Cathode for Room-Temperature Sodium-Ion Batteries. *Adv. Energy Mater.* **2013**, *3*, 156−160.
(35) Pan, H.; Lu, X.; Yu, X.; Hu, Y.-S.; Li, H.; Yang, X.-Q.; Chen, L. Sodium Storage and Transport Properties in Layered $Na_2Ti_3O_7$ for Room-Temperature Sodium-Ion Batteries. *Adv. Energy Mater.* **2013**, *3*, 1186−1194.
(36) Komaba, S.; Ishikawa, T.; Yabuuchi, N.; Murata, W.; Ito, A.; Ohsawa, Y. Fluorinated Ethylene Carbonate as Electrolyte Additive for Rechargeable Na Batteries. *ACS Appl. Mater. Interfaces* **2011**, *3*, 4165−4168.